Optimal frequency for Dynamic Wireless Power Transfer

Mincui LIANG, Khalil EL KHAMLICHI DRISSI, Christophe PASQUIER
Université Clermont Auvergne, Clermont Auvergne INP, CNRS, Institute Pascal
Campus Universitaire des Cézeaux, 4 Avenue Blaise Pascal
Aubière France
Email: mincui.liang@uca.fr; khalil.drissi@uca.fr; christophe.pasquier@uca.fr;
URL: http://www.institutpascal.uca.fr/index.php/en/

Acknowledgments

Keywords

Abstract

To control the system for maximum power transfer, it is necessary to understand its behaviour for large range of frequencies. Based on the time domain theoretical analysis of a Series-Series compensated WPT, the optimal frequencies to reach maximum power are proposed, considering the misalignment between the primary and secondary coils. It is further validated by a simulation case study. The theoretical and simulation results match well.

Introduction

Transportation plays a critical role in achieving the net-zero emission goal as it is responsible for 17% of greenhouse gas emissions. Therefore, The COP26 suggested that countries and states should accelerate the transition to zero-emission vehicles in 10 years. Consequently, the sales of global zero-emission vehicles are projected to increase approximately by 70% in 2040 [1]. Electric Vehicles (EVs) are the most mature zero-emission vehicle technology. As the demand for EVs increases, the need for transport infrastructures and supplementary facilities will increase correspondingly, especially power transfer systems for charging.

Power transfer systems can be classified into wired power transfer and Wireless Power Transfer (WPT). Compared to wired power transfer, WPT is safer and can seamlessly integrate with autonomous connection in the future. Practically, WPT has two main applications for EVs, static charging and dynamic charging. Dynamic Wireless Power Transfer (DWPT) not only inherits the advantages of WPT but also can solve the well-known battery range limitations by reducing the size of the battery and charging it while driving. Although DWPT is not yet mature for the commercial use, many DWPT system prototypes using magnetic resonance technology exist [2]. This research focus on magnetic resonant coupling DWPT technology. However, there are a few challenges of designing the controller for a dynamic magnetic resonance DWPT system. On the one hand, adding a resonant tank as a compensation network can increase the quality factor and thus amplify the power transfer. On the other hand, it also makes the system sensitive to misalignment, which causes a significant reduction in efficiency with respect to the transmission distance. Precisely, the main reason why DWPT is more difficult to control than the static

WPT is that sensitive parameters, like coupling coefficient k, are not fixed since the lateral and vertical displacements of EVs vary. Thus, it is essential to investigate the potential influences of those sensitive parameters on the behaviour of the DWPT systems so as to control the systems for maximum power transfer.

This paper aims to provide a holistic overview of the current progress and trend in the WPT and propose a novel method to identify the optimal operating frequencies for the DWPT. Specifically, it is organized in a logical order as follows: 1) to review the Series-Series compensated WPT (SS-WPT) which topology is considered sufficient for modelling the DWPT at the first stage, 2) to review operating frequencies for the WPT, 3) to construct a theoretical model for finding those optimal frequencies to reach maximum power transfer with respect to different coupling coefficients of misalignment, and 4) to carry out a case study using the developed theoretical model and validate the system performances using dynamic simulation.

Series-series compensated WPT

There are four mono-resonant converter topologies of compensation circuits for WPT applications, i.e. Series-Series (SS), Series-Parallel (SP), Parallel-Parallel (PP) and Parallel-Series (PS). Other topologies use different combinations of multi-inductor and multi-capacitor components designed for better performance and for larger power transmission. SS topology is the most straightforward and favourable solution to achieve Maximum Wireless Power Transfer (Max-WPT) and guarantee high efficiency. Misalignment and frequency bifurcation phenomenon are two main challenges of the DWPT systems [3]. From the circuit theory perspective, the SS topology is adequate to address the challenges. SS topology design is load-impedance-independent and mutual-inductance-independent for various misalignment situations [4]. Besides, SS topology can reduce the voltage rating of the power supply to reduce losses [5]. Furthermore, the current source-type primary series–secondary series (I-SS) topology has a k-independent feature in terms of maximum power transfer, high power efficiency and load independent output characteristics [2]. Therefore, SS topology is sufficient to test the proposed controller at the first stage. A simple SS-WPT compensation network, consisting of the primary side with a DC/AC converter, the wireless link and the secondary side with a resistive load, is considered during this study, as shown in Fig. 1. The switching strategy applied to the DC/AC converter corresponds to 1) SW1 and SW4 are on and SW2 and SW3 are off for the first half period, $0 < t < \frac{T}{2}$, and 2) SW2 and SW3 are on and SW1 and SW4 are off for the second half period, $\frac{T}{2} < t < T$. At this stage, Power Factor Corrector (PFC) and DC/DC on-board charger are not considered.
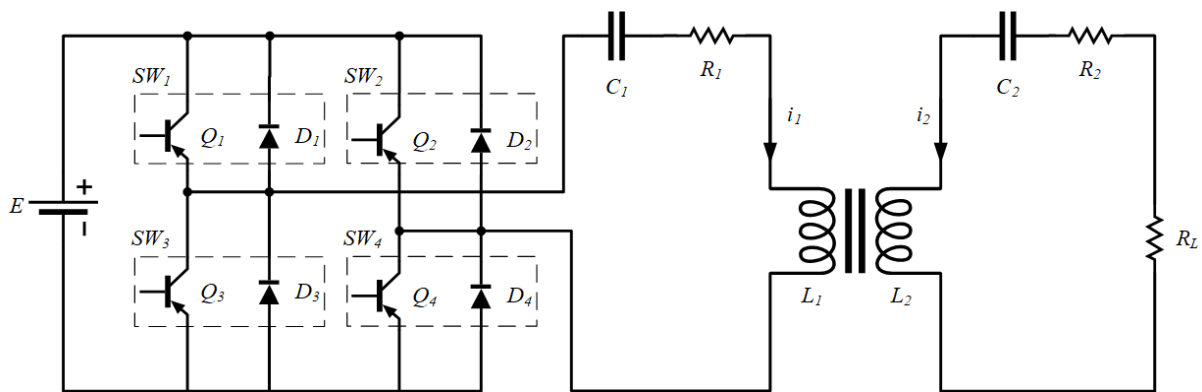

Fig. 1: Circuit diagram of a series-series WPT compensation network

Switching frequencies for DWPT

Practically, switching frequencies for DWPT vary depending on the control aims of the system. It is preferable to maintain the system operation when input voltage and input current are in phase to reduce the electrical stress on semiconductor devices and thus reduce switching losses, known as soft switching. The optimal frequencies of the Zero Voltage Switching (ZVS) [6] control is for high power transfer.

In [7], the optimal frequency of the proposed Maximum Energy Efficiency Tracking method is slightly lower than the resonance frequency. In this paper, the optimal frequency is the frequency corresponding to the maximum power point of input or its corresponding output power. We named it as Maximum Power Point Frequency (MPPF). There are several MPPFs in the SS-WPT system for different coupling coefficients. According to the IEC 61980-3 standard, the switching frequency of the WPT systems for EVs is between 79 kHz to 90 kHz [8]. It is considered as a high control frequency for power electronics and a narrow operation frequency range. From our point of view, following the IEC 61980-3 standard, the best choice is the MPPF below the primary resonance frequency, reducing the switching losses and maximizing the transferred power.

Theoretical modeling of the SS-WPT

In this section, a theoretical model of the SS-WPT is thoroughly presented in order to understand how different parameters correlate and affect the system performances. Fig. 2 (a) gives an equivalent circuit of the SS-WPT compensation network presented in Fig. 1. Two current-controlled voltage sources are introduced to represent the mutual inductance transformer, with two corresponding currents i_1 and i_2.
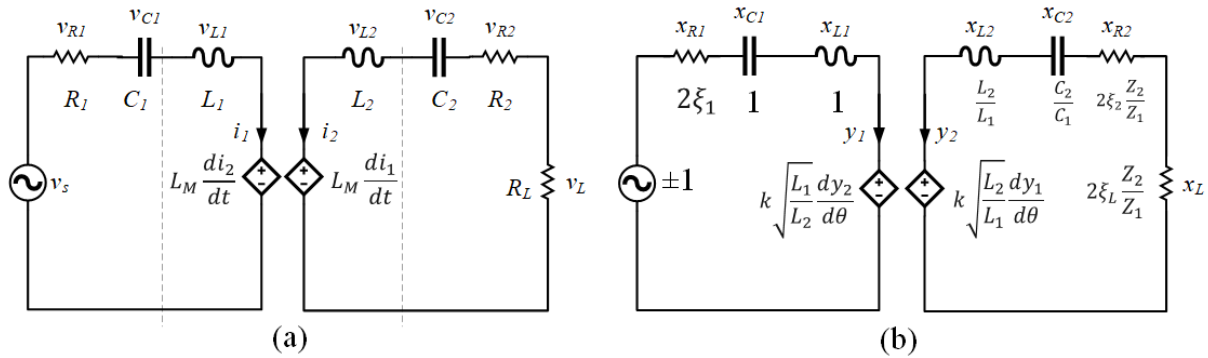

Fig. 2: (a) SS-WPT equivalent circuit with current-controlled voltage source; (b) Corresponding circuit with dimensionless elements

The mathematical relationship in time domain is given below in (1). The equivalent main voltage source $v_s = E$ when $0 < t < \frac{T}{2}$ and $v_s = -E$ when $\frac{T}{2} < t < T$. T is the switching period and t is the operating time.

$$
\begin{cases}
v_s = v_{C1} + R_1 i_1 + v_{L1} + L_M \frac{di_2}{dt} \\
0 = v_{C2} + (R_2 + R_L)i_2 + v_{L2} + L_M \frac{di_1}{dt} \\
i_1 = C_1 \frac{dv_{C1}}{dt} \\
i_2 = C_2 \frac{dv_{C2}}{dt}
\end{cases}
\tag{1}
$$

By applying theoretical modelling, the system can reach almost 100% efficiency, assuming losses are negligible and all semiconductor devices are ideal. The theoretical model does not include the model of the switching losses. However, the switching losses need to be considered since the finding of the optimal operational frequency is not based on Zero Current Switching (ZCS) control strategy. Therefore, an equivalent resistor is introduced to include the switching losses in the model, which is equal to 5 times of the coil losses on each side. The resistor of each designed coil using litz wire is 0.03 Ω in our setup, and hence we put two equivalent resistors (0.15 Ω each) on both sides to represent the switching, capacitor and coil losses. This value will be adapted according to our setup. The efficiency is then lower than one and close to the real situation.

SS-WPT model with dimensionless elements

For the ease of analysis and representation in phase plane, the model uses dimensionless elements, which are scalable and can be adjusted for any input source, coil parameters, compensation capacitors and re-

Table I: Dimensionless and corresponding not-dimensionless elements of the model

Elements	Voltage	Current	Resistor	Time	Inductor	Capacitor
Not-dimensionless	$v_{C_1}, v_{C_2}, v_s, v_L$	i_1, i_2	R_1, R_2, R_L	t	$L_{1,2}$	$C_{1,2}$
Dimensionless	x_1, x_2, u, x_L	y_1, y_2	$2\xi_1, 2\xi_2, 2\xi_L$	$\frac{\theta}{\omega_{r1}}$	1	1

sistive loads. The equivalent dimensionless circuit diagram is given in Fig. 2 (b). Parameters of dimensionless and not-dimensionless elements are defined in Table I. Additionally, the switching frequency is $f = \frac{1}{T} = \frac{\omega}{2\pi}$. The normalized or dimensionless angular frequency is $\omega_n = \frac{\omega}{\omega_{r1}}$, where $\omega_{r1} = 2\pi f_{r1}$ and $\omega_{r2} = 2\pi f_{r2}$. More specifically, the angular frequencies of the primary and secondary circuits are $\omega_{r1} = \frac{1}{\sqrt{L_1 C_1}}$ and $\omega_{r2} = \frac{1}{\sqrt{L_2 C_2}}$ respectively. The characteristic impedance in the primary and secondary circuits are $Z_1 = \sqrt{\frac{L_1}{C_1}}$ and $Z_2 = \sqrt{\frac{L_2}{C_2}}$ respectively. The mathematical model with dimensionless elements is given below in (2). $\theta = \omega_{r1} t$, when $0 < \theta < \frac{\pi}{\omega_n}$, $u = 1$; when $\frac{\pi}{\omega_n} < \theta < \frac{2\pi}{\omega_n}$, $u = -1$.

$$\begin{cases} u = x_1 + 2\xi_1 y_1 + \frac{dy_1}{d\theta} + kn\frac{dy_2}{d\theta} \\ 0 = \frac{x_2}{n^2} + a(2\xi)y_2 + \frac{dy_2}{d\theta} + \frac{k}{n}\frac{dy_1}{d\theta} \\ y_1 = \frac{dx_1}{d\theta} \\ y_2 = \frac{1}{(an)^2}\frac{dx_2}{d\theta} \end{cases} \tag{2}$$

where, n is the ratio of the turns of two inductors, $n = \sqrt{\frac{L_2}{L_1}}$; $(an)^2$ is the ratio of two capacitors, $(an)^2 = \frac{C_1}{C_2}$; a is the ratio of two resonance frequency, $a = \frac{\omega_{r2}}{\omega_{r1}}$; an^2 is the ratios of primary and secondary impedance, $an^2 = \frac{Z_2}{Z_1}$; k is the coupling coefficient; ξ is the sum of dimensionless resistors on secondary side, $\xi = \xi_2 + \xi_L$; $x_{1,2}$ is dimensionless voltage of C_1 and C_2, $x_{1,2} = \frac{v_{C_{1,2}}}{E}$; $y_{1,2}$ is dimensionless current of L_1 and L_2, $y_{1,2} = \frac{Z_1}{E}i_{1,2}$; P is dimensionless power, p is real power, $P_0 = \frac{E^2}{Z_1}$, $P = \frac{p}{P_0}$.

To transform the model (2) into a state space equation in (3), we get, when $0 < \theta < \frac{\pi}{\omega_n}$,

$$\begin{bmatrix} \dot{y}_1 \\ \dot{y}_2 \\ \dot{x}_1 \\ \dot{x}_2 \end{bmatrix} + \begin{bmatrix} \frac{2\xi_1}{1-k^2} & \frac{-2\xi kna}{1-k^2} & \frac{1}{1-k^2} & \frac{-k}{n(1-k^2)} \\ \frac{-2\xi_1 k}{n(1-k^2)} & \frac{2\xi a}{(1-k^2)} & \frac{-k}{n(1-k^2)} & \frac{1}{n^2(1-k^2)} \\ -1 & 0 & 0 & 0 \\ 0 & -(an)^2 & 0 & 0 \end{bmatrix} \begin{bmatrix} y_1 \\ y_2 \\ x_1 \\ x_2 \end{bmatrix} = \begin{bmatrix} \frac{1}{1-k^2} \\ \frac{-k}{n(1-k^2)} \\ 0 \\ 0 \end{bmatrix} \tag{3}$$

which is equivalent to $\dot{X} + AX = B$, where

$$A = \begin{bmatrix} \frac{2\xi_1}{1-k^2} & \frac{-2\xi kna}{1-k^2} & \frac{1}{1-k^2} & \frac{-k}{n(1-k^2)} \\ \frac{-2\xi_1 k}{n(1-k^2)} & \frac{2\xi a}{(1-k^2)} & \frac{-k}{n(1-k^2)} & \frac{1}{n^2(1-k^2)} \\ -1 & 0 & 0 & 0 \\ 0 & -(an)^2 & 0 & 0 \end{bmatrix} ; B = \begin{bmatrix} \frac{1}{1-k^2} \\ \frac{-k}{n(1-k^2)} \\ 0 \\ 0 \end{bmatrix}$$

and X is state vector, A is system matrix, and B is control matrix. By solving the state space equation (3), one derives the state vector, X. It contains the dimensionless variation of the primary inductor current, y_1, the secondary inductor current, y_2, the primary capacitor voltage, x_1 and the secondary capacitor voltage, x_2. Those variables are important for the state plane analysis and for the energy tank and power evaluation.

Power representation

The input power is the total power supplied by the DC source and expressed as the mean value of the input current multiplying by the DC voltage. The dimensionless input power is equal to the mean value of y_1 for a half period multiplying by the dimensionless DC source, 1. Since there is a relationship

between two half periods when reaching steady state for all variables, $X(t) + X(t + \frac{T}{2}) = 0$, it thus only needs to evaluate the primary dimensionless coil current and dimensionless input voltage.

The definition of the dimensionless input power is given in (4).

$$P_{input} = 1 * \bar{y_1} = \frac{\omega_n}{\pi} \int_0^{\frac{\pi}{\omega_n}} y_1(\theta) d\theta \tag{4}$$

The output power is the power consumed by the resistive load and expressed as the mean value of the square of the output current multiplying by the value of the resistive load. For the dimensionless output power, it expresses as the mean value of the square of y_2, which is $\bar{y_2}^2$. The half period is sufficient to determine this mean value. Multiplying this mean value by the dimensionless load resistor, $2\xi_L$, we get the dimensionless output power,

$$P_{output} = 2\xi_L * \bar{y_2}^2 = 2\xi_L * \frac{\omega_n}{\pi} \int_0^{\frac{\pi}{\omega_n}} y_2^2(\theta) d\theta \tag{5}$$

The definition of the efficiency of the SS-WPT system is given in (6).

$$\eta = \frac{P_{output}}{P_{input}} \tag{6}$$

Case study

A 7.4 kW SS-WPT compensation network

In this section, a 7.4 kW SS-WPT compensation network is represented using the developed theoretical modelling method and validated against the dynamic simulation results. The values of the system variables used in this model for theoretical modeling and simulation are given in Table II. The different misalignment situations with different coupling coefficients ($k = 0.1$ to 0.9) are investigated so as to reach optimal frequencies for each k and to ensure a Maximum Wireless Power Transfer.

Table II: Parameter specification of system components

$C_1, C_2(nF)$	$L_1, L_1(\mu H)$	Power (kW)	Q	f_r (kHz)	Z_c (Ω)	R_1, R_2(Ω)	R_L (Ω)	E(V)
33	82.5	7.4	5	96.5	50	0.3	10	302

The theoretical results show that the input power and output power largely depend on the normalized switching frequency, ω_n, and the coupling coefficient, k. Fig. 3 presents the relationships between the input and output power and these two parameters. When k is below 0.3, a significant maximum power point is reached. Specifically, when the normalized frequency is equal to 1 and k is at 0.1, the input
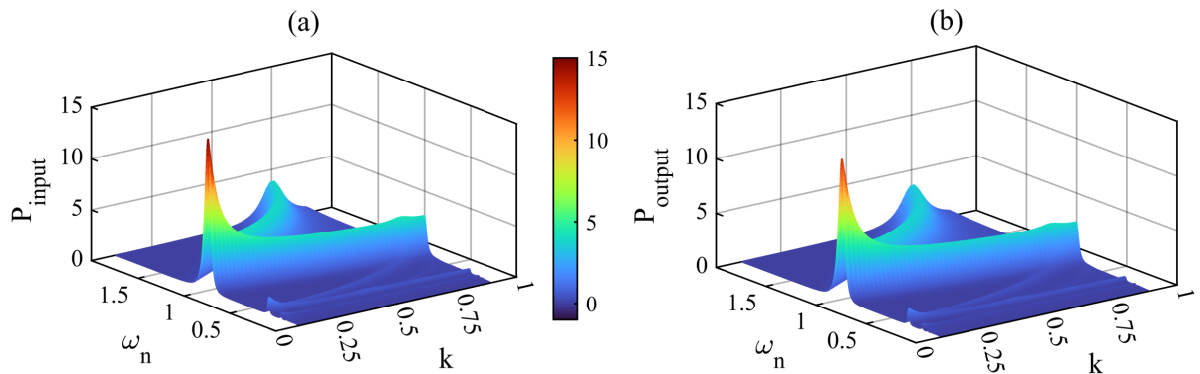

Fig. 3: Dimensionless power for normalized frequencies and corresponding k: (a) P_{input} ; (b) P_{output}

power and output power reach the global maximum. When k is higher than 0.3, the peak power point is almost constant.

Fig. 4 gives a closer look at how the input power and output power interact with the normalized switching frequencies ($0 < \omega_n < 2$) and the coupling coefficients ($k = 0.1$ to 0.9). The envelope of the power curves indicates the maximum power points corresponding to their switching frequencies, MPPFs, and coupling coefficients, with highlighted optimal power peaks.
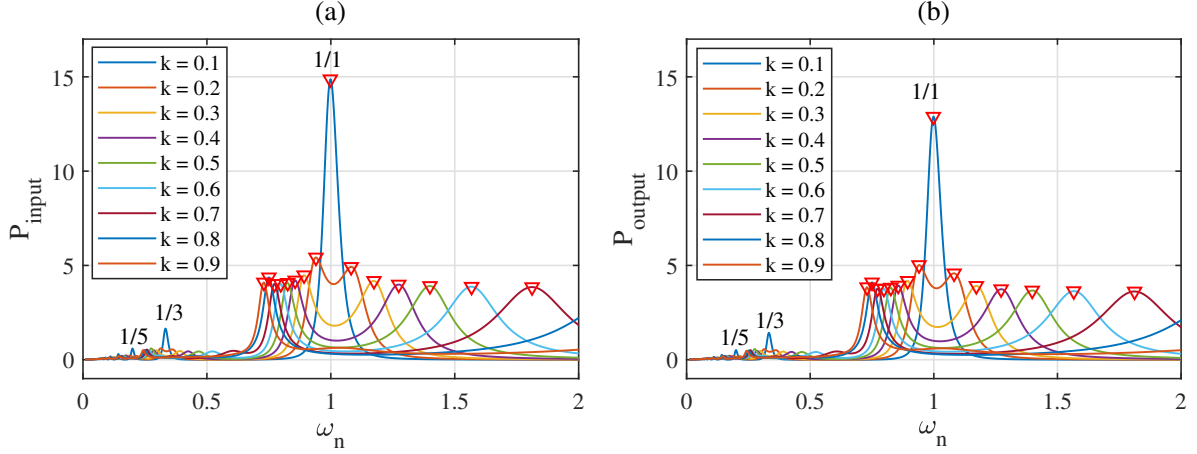

Fig. 4: Dimensionless power against ω_n for different k: (a) P_{input}; (b) P_{output}

Fig. 5 uses phase planes to represent the highlighted peak power points in Fig. 4 with respect to their corresponding MPPFs and coupling coefficients. Specifically, Fig. 5(a) - (c) correspond to the peak input power cases in Fig. 4 (a). Fig. 5(a) shows the corresponding MPPF and coupling coefficient for each peak input power point, which are highlighted with respect to the MPPFs in blue ($\omega_n < 1$) and red ($\omega_n > 1$). Fig. 5 (b) and (c) draw phase planes to show the peak input powers for the MPPFs lower or higher than 1, respectively. The cases with respect to the peak output power points, corresponding to Fig. 4 (b), are shown similarly in Fig. 5(d) - (f). When the resonance system is symmetric, meaning L_1 is equal to L_2 and C_1 is equal to C_2, the MPPFs of the maximum input power and maximum corresponding output power are very close. As seen in Fig. 5, the energy tank levels, operating at normalized frequency lower than 1, are generally higher than operating at normalized frequency higher than 1. It is thus straightforward to use Fig. 5 to select the switching frequency according to the physical limitation of the energy tank.

Fig. 6 shows the maximum input power and maximum output power differences and their transferring efficiencies, with respect to their MPPFs and corresponding coupling coefficients. For the peak power point, it can choose to operate at normalized frequency lower than 1 or higher than 1. Specifically, when k is moving from 0.1 to 0.3, the peak power input and output drops dramatically, indicating significant changes in power. When k is larger than 0.3, the power starts to reach a similar power level for both normalized frequency ranges. It means that operating at normalized frequency lower than 1 has the similar performance as higher than 1. It is thus preferable to operate the systems with a normalized MPPF lower than 1 since lower frequency has less demand on the component selection than higher frequencies. The two green line represent the efficiency of the system at switching frequency lower or higher than 1. From 0.1 to 0.2, the system can deliver maximum input and output power but with the lowest efficiency. When k is increasing, the input and output power and operating efficiency are similar for both MPPF ranges. However, the system performs slightly better in efficiency when the switching frequency is higher than 1, and a little better in maximum input and output power when the frequency is smaller than 1. When losses are lower, the differences get smaller, corresponding to higher efficiency. The maximum output power depends on the resistive load without considering losses. The definition of the maximum output power is given in (7).
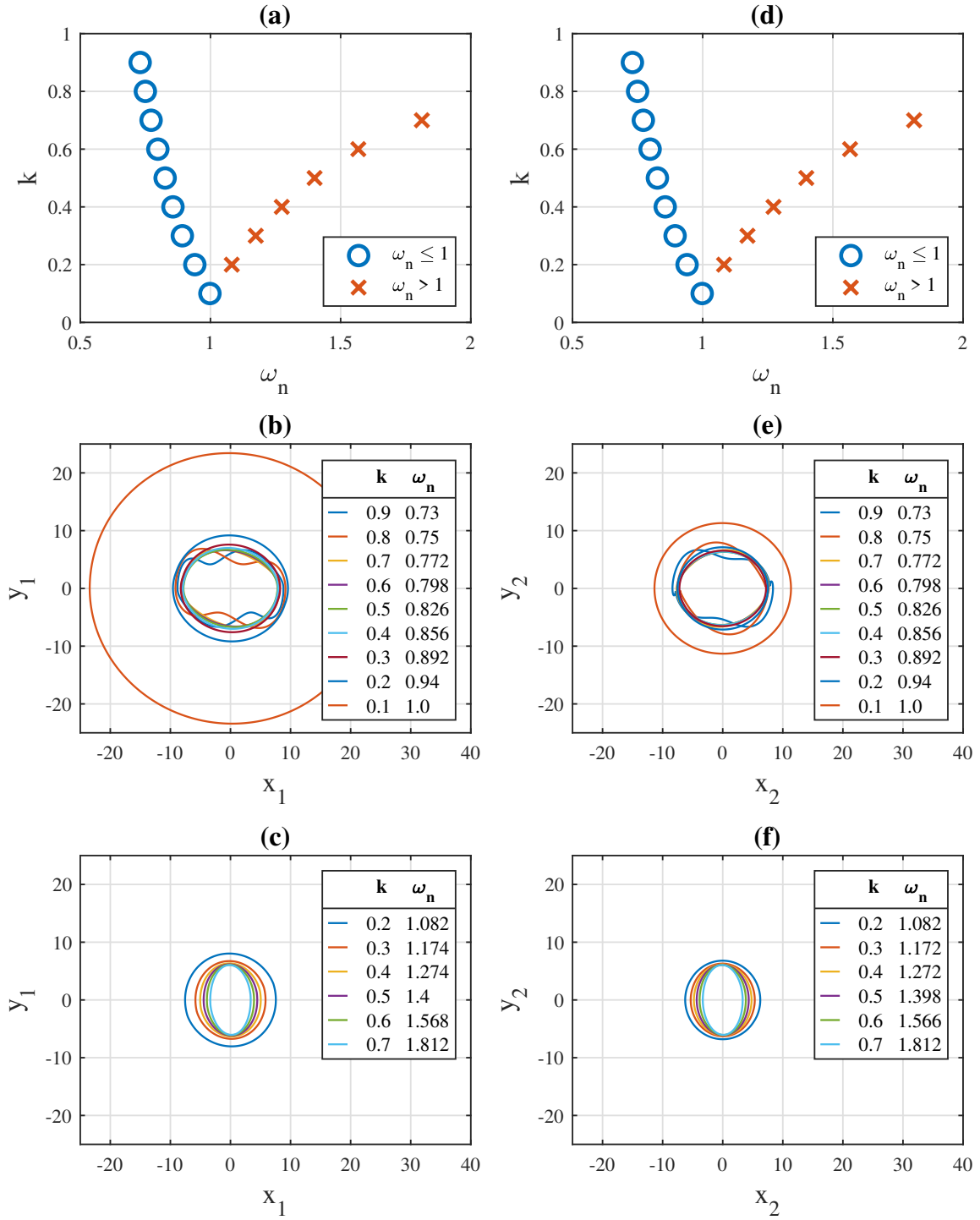
$$P_{max} = \frac{8}{\pi^2} \frac{(nE)^2}{R_L} \tag{7}$$

Fig. 5: MPPF and corresponding *k* and their phase plane : (a) ω_n and *k* for maximum P_{input} ; (b) Corresponding phase plane ($\omega_n <= 1$) for (a) ; (c) Corresponding phase plane ($\omega_n > 1$) for (a) ; (d) ω_n and *k* for maximum P_{output} ; (e) Corresponding phase plane ($\omega_n <= 1$) for (d) ; (f) Corresponding phase plane ($\omega_n > 1$) for (d)
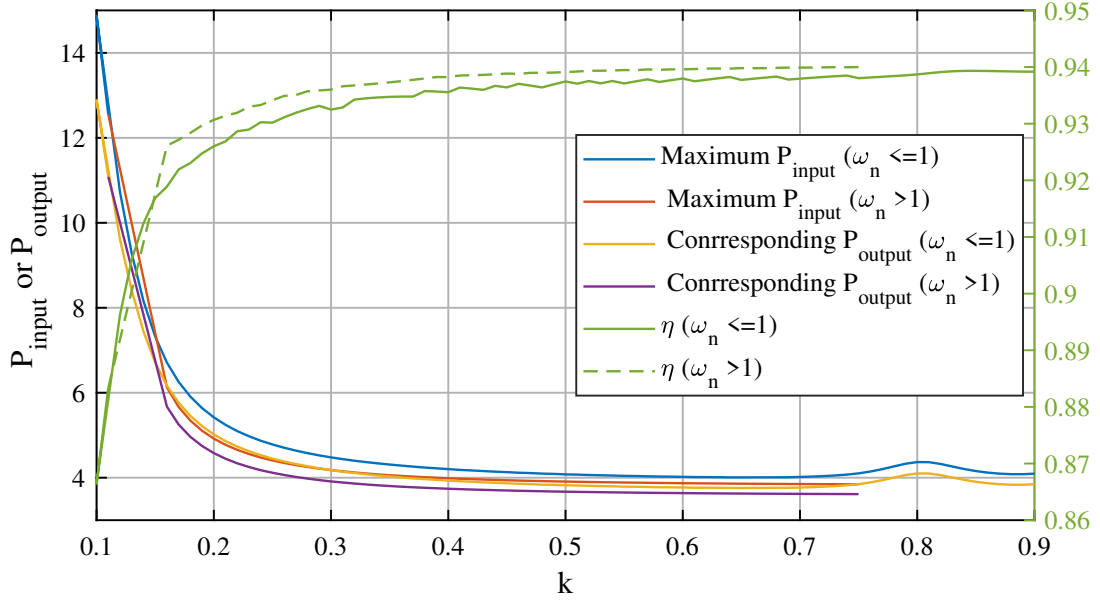
Fig. 6: Maximum power and efficiency for dimensionless P_{input} and P_{output}

MPPFs corresponding to the maximum input power and maximum corresponding output power are load dependent. However, differences between their MPPFs are minor and are getting smaller when k is increasing, as shown in Fig. 7. Table III further specifies the Normalised Root Mean Square Error (NRMSE) for the dataset of Fig. 7 (a). When k is equal to 0.1, the difference is the biggest and the value is less than 1%. Similar conclusions can be drawn for Fig. 7 (b).
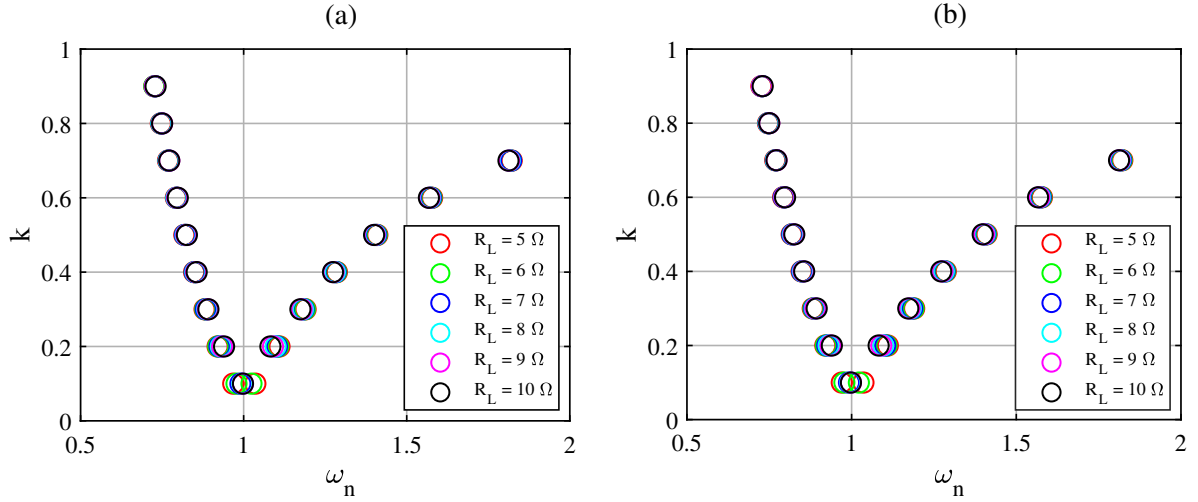

Fig. 7: MPPFs for different resistive loads : (a) MPPFs for maximum input power; (b) MPPFs for maximum output power

Table III: NRMSE of MPPFs for different resistive loads for maximum input power

k	0.1	0.2	0.3	0.4	0.5	0.6	0.7	0.8	0.9
NRMSE (%)	0.985	0.745	0.441	0.299	0.264	0.210	0.174	0.170	0.175

Note: NRMSE - Normalised Root Mean Square Error, $NRMSE = \frac{RMSE}{\bar{O}}$, where $\bar{O}$ is the mean value of the dataset

Simulation and validation

A Simulink model is developed to simulate and validate the performances of the SS-WPT in Fig. 1, with respect to the normalized frequency from 0.5 to 1.6 and the coupling coefficients from 0.1 to 0.6, as the difference is negligible, when coupling coefficient is higher than 0.6. In Fig. 8, the red stair line represents normalized switching frequency scenarios used in the simulation. The color of each power line corresponds to different coupling coefficient from 0.1 to 0.6. It can be seen that, at primary resonance frequency ($\omega_n = 1$ and $k = 0.1$), it has the global maximum input power. When k increases, the frequency bifurcation phenomenon becomes obvious especially for the situations where primary and secondary resonance tank elements are the same. It is clear that the simulation results and the theoretical results in Fig. 4 agreed very well, which can be further speculated in Fig. 8.
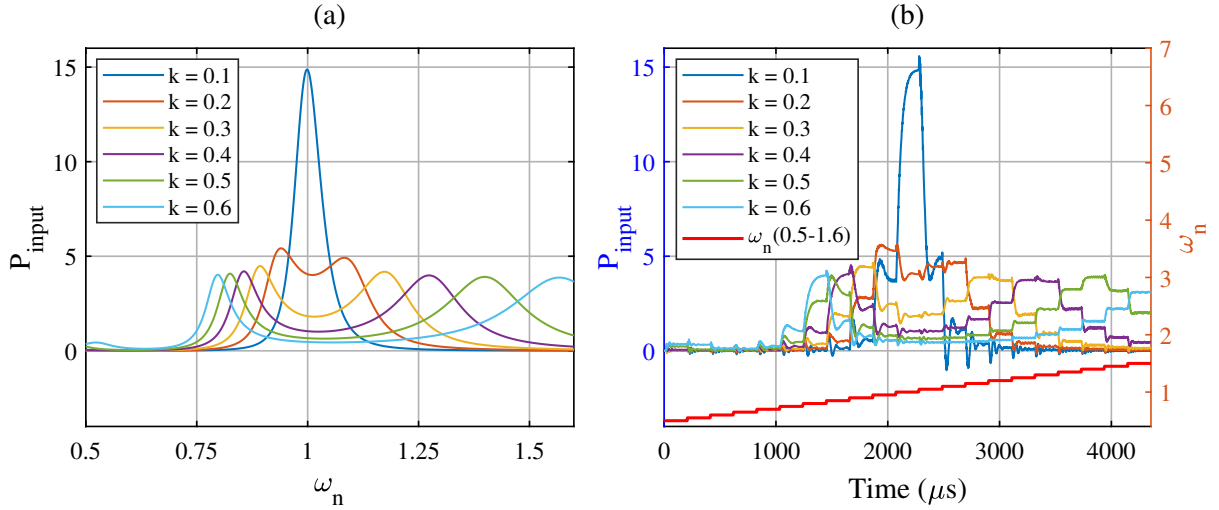

Fig. 8: Result comparison: (a) Theoretical results; (b) Simulation results

In order to evaluate optimal frequencies for each coupling coefficient, the simulation model in time domain was run repeatedly for each k from 0.1 to 0.6 and a range of frequencies from 0.5 to 1.6 including the optimal frequencies representing the dynamic behavior for each given frequency. The simulation model includes 21 normalized angular frequencies (ω_n) between 0.5 to 1.6, plotted as a red stair line in Fig. 8 (b). The simulation runs at each given frequency for 207 μs and reaches the steady state. The results in Fig. 8 give the input power from 0 to 207 μs for each given frequency. The maximum input power at steady state can be found at the corresponding MPPF for each k.

The results presented in Table IV further prove an excellent agreement between the theoretical and sim-

Table IV: Simulation and theoretical results for maximum input power

k	0.6	0.5	0.4	0.3	0.2	0.1	0.2	0.3	0.4	0.5	0.6
MPPF	0.80	0.83	0.86	0.89	0.94	1.0	1.08	1.17	1.27	1.40	1.57
Theor. P_{in}	4.02	4.08	4.20	4.48	5.42	14.87	4.92	4.18	3.99	3.91	3.87
Sim. P_{in}	3.90	3.90	4.03	4.40	5.19	14.29	4.84	4.04	3.88	3.8	3.70
NRMSE (%)	1.51	2.23	2.10	0.87	2.16	2.00	0.83	1.71	1.33	1.41	2.26
Theor. P_{out}	3.77	3.82	3.93	4.18	5.02	12.89	4.58	3.91	3.74	3.67	3.64
Sim. P_{out}	3.70	3.70	3.70	4.10	4.84	11.70	4.36	3.69	3.53	3.45	3.38
NRMSE (%)	0.94	1.64	3.04	0.95	1.85	4.82	2.42	2.91	2.95	3.10	3.67
Theor. η	0.94	0.94	0.94	0.93	0.93	0.87	0.93	0.94	0.94	0.94	0.94
Sim. η	0.95	0.95	0.92	0.93	0.93	0.82	0.9	0.91	0.91	0.91	0.91
NRMSE (%)	0.64	0.67	0.84	0.08	0.22	2.76	1.68	1.19	1.53	1.57	1.60

Note: P_{in} - Input power; P_{out} - Output power ; Theor. - Theoretical; Sim. - Simulation

ulation results. As the theoretical modeling results in higher efficiency, larger equivalent resistor losses on both sides were introduced to better present and compare the results. Furthermore, if the system can avoid operating at the global maximum power point, the normalized output power is almost constant and the resistive loads have little effect on the MPPFs. Without considering the global maximum point when k is equal to 0.1, the theoretical normalized average output power is 4.03 which is equivalent to real output power of 7.34 kW. For our case study with 7.4 kW output power, the SS-WPT system achieve excellent performances when operating at the selected optimal frequencies.

Conclusion

Series-Series compensation topology has the potential to reach maximum wireless power transfer and high efficiency under different misalignment conditions. A time-domain theoretical study of an SS-WPT compensation network is conducted so as to find Maximum Power Point Frequencies (MPPFs) for maximum power transfer of a DWPT system with different coupling coefficients. An excellent agreement is noticed between the theoretical and simulation results during validation. Based on the phase plane analysis, it is easy to normalize constraints of various components in terms of maximum voltages and currents necessary for the right choice of the passive and active components of the SS-WPT. Under steady-state conditions, the method facilitates qualitative understanding of system operation including identification of the operating modes. In the future research, different control strategies are to be developed to reach the MPPFs and allows the system to operate at maximum power points for any misalignment conditions.

References

[1] United Nations, "Transport," UN Climate Change Conference (COP26) at the SEC – Glasgow 2021, 16-Sep-2021. [Online]. Available: https://ukcop26.org/transport/. (Accessed: 15-Nov-2021).

[2] Chun T. Rim; Chris Mi, "Introduction to Dynamic Charging," in Wireless Power Transfer for Electric Vehicles and Mobile Devices, IEEE, 2017, pp.155-160, doi: 10.1002/9781119329084.ch8.

[3] A. Triviño-Cabrera and J. Sánchez, "A Review on the Fundamentals and Practical Implementation Details of Strongly Coupled Magnetic Resonant Technology for Wireless Power Transfer," Energies, vol. 11, no. 10, p. 2844, Oct. 2018.

[4] Triviño-Cabrera, A., González-González, J.M., Aguado, J.A. (2020). Wireless Chargers for Electric Vehicles. In: Wireless Power Transfer for Electric Vehicles: Foundations and Design Approach. Power Systems. Springer, Cham. https://doi.org/10.1007/978-3-030-26706-32

[5] K. Aditya and S.S. Williamson, "Comparative study of series–series and series–parallel compensation topologies for electric vehicle charging," in 2014 ISIE Conf., pp. 426–430.

[6] Y. Jiang, L. Wang, Y. Wang, J. Liu, M. Wu and G. Ning, "Analysis, Design, and Implementation of WPT System for EV's Battery Charging Based on Optimal Operation Frequency Range," in IEEE Transactions on Power Electronics, vol. 34, no. 7, pp. 6890-6905, July 2019, doi: 10.1109/TPEL.2018.2873222.

[7] W. X. Zhong and S. Y. R. Hui, "Maximum Energy Efficiency Tracking for Wireless Power Transfer Systems," in IEEE Transactions on Power Electronics, vol. 30, no. 7, pp. 4025-4034, July 2015, doi: 10.1109/TPEL.2014.2351496.

[8] Electric vehicle wireless power transfer (WPT) systems - Part 3: Specific requirements for the magnetic field wireless power transfer systems, IEC 61980-3 ED1, 2020